On the Energetics of a Switchable Parallel Elastic Actuator Design for Monopedal Running

Xin Liu and Ioannis Poulakakis

***Abstract*— Switchable Parallel Elastic Actuators (S-PEAs) represent a novel way for introducing compliant elements in legged robots. This paper investigates the energetic effects of a S-PEA design on running gaits in the context of the monopedal robot SPEAR, which has its knee driven by a S-PEA. In our implementation of the S-PEA concept, a mechanical switch located at the foot engages the spring during stance to store energy and disengages it during flight to allow for precise control of the leg's configuration without interfering with the spring. Parameter optimization indicates that the S-PEA configuration outperforms common Parallel Elastic Actuator (PEA) designs by $10-20\%$ in both hopping-in-place and hopping-forward gaits, and this advantage increases to about 40% at higher running velocities. It is deduced that the ability of SPEAR to adjust the effective stiffness of the leg without requiring additional energy, by simply changing the knee angle prior touchdown, explains part of this advantage.**

I. Introduction

One of the main reasons for exploring the use of legs for robotic locomotion is mobility [1]. In addition to mobility however, energy efficiency is an important consideration for deploying these robots in the field [2]. The design of energy efficient legged robots is challenging due to the nature of the motion [3]. During walking and running, the gravitational potential energy and kinetic energy of the center of mass as well as the kinetic energy of the limbs fluctuate within a stride. Biomechanical studies of human and animal locomotion indicate that compliant elements – such as tendons and muscles – play important roles in reducing the energetic cost of walking and running motions. By storing part of the mechanical energy in the deformation of muscle fibers and tendons and releasing it at a later part of the gait, cyclic motions can be sustained without excessive effort [4].

Inspired by nature, compliant elements have been introduced to legged robots to improve their energetic performance. Series Elastic Actuators (SEAs) represent one way to incorporate compliance in a robot's structure [5]. Instead of connecting the actuator directly to a robot's limb, a compliant element is placed in between to filter impulsive loads and store energy. Several robots have been designed using SEAs; the bipedal robot MABEL [6] is an example. However, SEAs increase the number of degrees of freedom (DOF) of the system, and render controller design more challenging. Most important, the actuator needs to produce forces or torques that have the same magnitude as those developed by the spring [7]. To most electrically driven robots, this means energy consumption even when a robot is just standing still.

This work is supported in part by NSF grants CMMI-1130372, IIS-1350721 and ARO contract W911NF-12-1-0117.

The authors are with the Department of Mechanical Engineering, University of Delaware, DE, USA; {xinliu, poulakas}@udel.edu

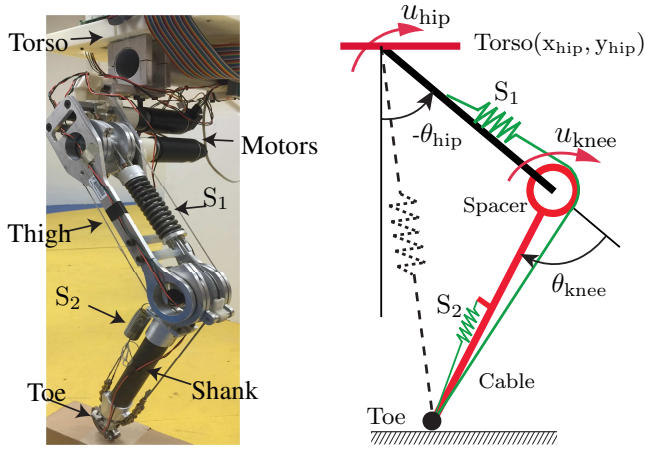

Fig. 1. (a) The monopedal robot SPEAR [8]. (b) A schematic of SPEAR. One end of the energy-storing spring S_1 is attached to the thigh, while the other end is attached to the shank via the soft spring S_2. A mechanical switch placed at the toe, engages S_1 during stance to store energy as the knee compresses.

Parallel Elastic Actuator (PEA) designs provide an alternative way to introduce compliance. In contrast to SEAs, the elastic element is placed in parallel with the motor [9]. Simulation studies indicate that PEAs reduce both power and torque requirements in bipedal walking and running gaits [10], as well as in quadrupedal bounding gaits [11]. However, the spring in typical PEA configurations limits the range of joint motion and may thus reduce mobility [7], [12].

Recently, the concept of a *Switchable Parallel Elastic Actuator* (S-PEA) has been used to overcome the disadvantages of PEA designs [12]. A switch is used to engage the parallel spring when energy storage is desired and disengage it to avoid impeding the joint motion [13]. Standalone S-PEA prototypes have been designed and tested in [7] and [12]. In the context of legged robots, the biped Phides incorporates elastic elements in series and in parallel with an actuator at its knee joints [14]. In [8], a the monopedal robot SPEAR is designed with a S-PEA actuating its knee joint. By placing a mechanical switch at the foot – see Fig. 1 and [8] for design details – the switching action of the parallel spring is naturally synchronized with the motion of the robot: the spring engages at stance due to ground reaction force and disengages when the leg is off ground.

This paper investigates the energetic effects of the S-PEA concept for running gaits using parameter optimization. Similarly to other parameter studies that explore SEA [15]

and PEA [16] designs, we consider monopedal hopping gaits that are generated by applying simple excitation commands to the actuators. Comparisons with alternative leg models – one that features a PEA and one that does not include compliance – demonstrate that the S-PEA outperforms both models in terms of energy consumption. It is deduced that the switchable compliance holds the key to gait efficiency, by allowing the effective stiffness of the leg during stance to be adjusted simply by changing the knee touchdown angle during flight, without incurring any additional energy cost.

II. The Monopedal Robot SPEAR

As shown in Fig. 1, SPEAR has four segments: a torso, a thigh, a shank and a toe [8]. The torso and thigh are connected by the hip joint, and the thigh and shank are connected by the knee joint. The toe is connected to the shank by a passive prismatic joint. To test the leg in planar hopping, the torso is constrained by a boom that allows SPEAR to move freely forward and backward as well as up and down; lateral leg movement and torso rotation are restricted. Both the hip and knee joints are actuated by DC motors. The inertia parameters of the leg are estimated and identified via experiments, and are given in Table I.

Fig. 1(b) presents a model of the S-PEA which drives the knee joint of SPEAR. During stance, the toe is pushed up by the ground reaction force to lock the lower end of the stiff spring S_1 to the shank, allowing energy storage. During the subsequent flight phase, the toe is released and S_1 is attached to the shank through the soft spring S_2, allowing the actuator to shorten or lengthen the leg without interfering with S_1. With the effect of the spring S_2 negligible, the torque developed at the (unilateral) rotational knee spring is

$$u_{\text{spring}} = \begin{cases} -56.67\max\{(\theta_{\text{knee}} - \theta_{\text{knee}}^{\text{TD}}), 0\}, & \text{if } y_{\text{toe}} = 0 \\ 0, & \text{if } y_{\text{toe}} > 0 \end{cases} \tag{1}$$

where $\theta_{\text{knee}}^{\text{TD}}$ is the knee angle at touchdown. It is emphasized that $\theta_{\text{knee}}^{\text{TD}}$ – which is freely prescribed during flight – determines the rest angle of the spring, thus providing an effective means for regulating leg stiffness.

TABLE I

Mechanical Parameters of the Leg

Parameter	Value	Units
Total mass (M)	6.71	kg
Torso mass (with boom and CPU) (M_0)	3.55	kg
Thigh mass (M_1)	2.43	kg
Shank mass (M_2)	0.73	kg
Thigh inertia (with reflected rotor inertia) (J_1)	0.06	kg m^2
Shank inertia (with reflected rotor inertia)(J_2)	0.02	kg m^2
Thigh length (L_1)	0.320	m
Shank length (L_2)	0.327	m
Thigh COM to hip distance $(L_{\mathrm{m},1})$	0.092	m
Shank COM to knee distance $(L_{\mathrm{m},2})$	0.097	m
Hip friction coefficient (f_1)	0.31	Nm/rad
Knee friction coefficient(f_2)	0.06	Nm/rad

III. Modeling SPEAR

In this section, a mathematical model of SPEAR for hopping is developed. As described in Section II, SPEAR has four degrees of freedom (DOF) when is in flight. Shown in Fig. 1(b), a convenient choice of generalized coordinates is[1] $q := (x_{\text{hip}}, y_{\text{hip}}, \theta_{\text{hip}}, \theta_{\text{knee}})'$, where $(x_{\text{hip}}, y_{\text{hip}})$ denote the Cartesian position of the hip, and $(\theta_{\text{hip}}, \theta_{\text{knee}})$ correspond to the hip and knee joint angles. The torso is kept horizontal by the boom, and its effect is represented by a point mass. As described in Fig. 2, a complete hopping cycle is composed by flight and stance phases. Switching occurs at touchdown (TD), liftoff (LO) and apex (APEX) events.

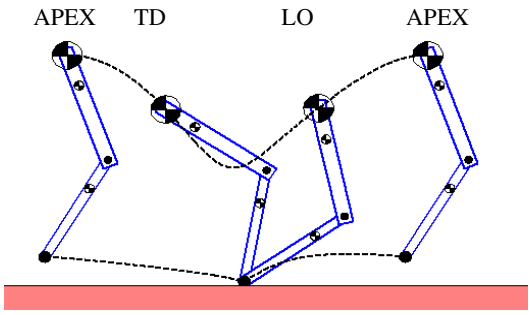

Fig. 2. A complete hopping gait that begins at the apex.

A. Floating-base Dynamics of the Leg

The dynamics of the system in floating base form is

$$\begin{aligned} D(q)\ddot{q} + C(q,\dot{q})\dot{q} + G(q) = \\ B(u_{\text{Act}} + u_{\text{Pas}} + u_{\text{Damp}}) + J'(q)F_{\text{ext}}, \end{aligned} \tag{2}$$

where D is the mass matrix, C contains Coriolis and centrifugal terms, G is the vector of gravity-dependent forces. The matrix B maps to the vector of generalized forces the active actuator torque $u_{\text{Act}} := (u_{\text{hip}}, u_{\text{knee}})'$, the joint viscous friction torque u_{Damp}, and the passive spring torque $u_{\text{Pas}} := (0, u_{\text{spring}})'$ computed by (1). Finally, J' is the transpose of the Jacobian matrix J mapping contact forces $F_{\text{ext}} = (F_{\text{ext}}^x, F_{\text{ext}}^y)'$ to the vector of generalized forces.

In stance, the toe-ground contact is modeled as a frictionless pin joint, resulting in the constraint $J\ddot{q} + \dot{J}\dot{q} = 0$, which together with equation (2) are used to compute the acceleration $\ddot{q}$ and contact force F_{ext}. In flight, F_{ext} is zero.

B. Event-based Transitions

1) Flight-to-stance Transition: The leg enters the stance phase when the height of the toe decreases to zero. The touchdown event is modeled as an inelastic instantaneous impact according to the assumptions in [17, Section 3.4].

2) Stance-to-flight Transition: The leg enters the flight phase when F_{ext}^y decreases to zero. Moreover, with the knee and hip joints actively controlled, liftoff can also be initiated by flexing the knee joint when the knee angle (as the leg extends) becomes equal to its touchdown value:

$$S_{\text{s}\to\text{f}} = \{x = (q', \dot{q}')' \mid F_{\text{ext}}^y = 0 \text{ or } \theta_{\text{knee}} = \theta_{\text{knee}}^{\text{TD}}\} \ . \tag{3}$$

[1]Notation: x' denotes the transpose of a vector $x \in \mathbb{R}^n$. Analogous notation is used for matrices.

3) Apex Event: A complete stride starts and ends when the hip joint reaches the apex height, when $\dot{y}_{\text{hip}} = 0$.

IV. Generation of Periodic Gaits

To explore the energetic effects of the S-PEA, a controller for generating periodic hopping is developed. The controller is considered successful if it can generate periodic gaits.

A. Stance Phase Excitation Function

Instead of specifying the desired motion of the hip and knee joints, the corresponding joint torques are commanded according to the prescription

$$u_i = a_0 + \sum_{k=1}^{5} a_k^i \sin(k\omega s) + b_k^i \cos(k\omega s), \tag{4}$$

for $i \in \{\text{hip}, \text{knee}\}$, where $s := t - t_{\text{TD}}$ is the stance time reset at the touchdown event. The motivation for prescribing torques instead of joint angles during stance is that the interaction forces between the leg and the ground are important. Furthermore, by parameterizing the torque directly, it is easier to compute motions that preserve leg compliance.

B. Flight Phase Excitation Function

During flight, PD control laws enforce the nominal joint angles $\bar{\theta}_{\text{hip}}$ and $\bar{\theta}_{\text{knee}}$ parameterized via Beziér polynomials

$$\bar{\theta}_i(s) = \sum_{k=0}^{5} c_k^i \frac{5}{k!(5-k)!}(s)^k(1-s)^{5-k}, \tag{5}$$

for $i \in \{\text{hip}, \text{knee}\}$, and s is the normalized time given by

$$s = \frac{t}{t_{\text{TD}}} \quad \text{or} \quad s = \frac{t - t_{\text{LO}}}{t_{\text{APEX}} - t_{\text{LO}}}. \tag{6}$$

C. Return Map

Taking the apex event to define the Poincaré section, a hopping gait naturally defines a return map $\mathcal{P}$, and

$$z[k+1] = \mathcal{P}(z[k], \alpha[k]) \ , \tag{7}$$

where $z := [y_{\text{hip}}, \theta_{\text{hip}}, \theta_{\text{knee}}, \dot{x}_{\text{hip}}, \dot{y}_{\text{hip}}, \dot{\theta}_{\text{hip}}, \dot{\theta}_{\text{knee}}]$ is the state at the apex – excluding the cyclic variable x_{hip} – and α includes all the parameters introduced by the stance and flight excitation functions. Then, the problem of finding periodic hopping gaits becomes equivalent to finding state vectors z and parameters α such that $z = \mathcal{P}(z, \alpha)$.

D. Cost Function

To provide cost functions that capture the energetic cost of hopping motions, we incorporate a simplified electric actuator model. It is assumed that the electric constant can be neglected and that each actuator can be modeled as an ideal torque source. Having the friction of the rotors lumped into the damping coefficient of the joints, the motor model takes the form

$$I_i = \frac{u_i}{n_i K_t} \quad \text{and} \quad V_i = \dot{\theta}_i n K_t + R I_i, \tag{8}$$

for $i \in \{\text{hip}, \text{knee}\}$, where V_i and I_i are the supply voltage and current of the motor, and n_i is the gearbox ratio (25:1 for the knee and 60:1 for the hip) joints [8]. The motor constant $K_t = 0.0414\text{Nm/A}$ and the resistance of the coil $R = 0.72\Omega$ are the same for both the hip and knee motors.

1) Cost of Hopping In-place: With the actuator model (8), the electrical energy consumed during the gait can be approximated as in [16] by

$$\begin{aligned} c_{\text{ele}} &= \sum \int_0^T \max\{(V_i I_i), 0\} dt \\ &= \sum \int_0^T \max\{(I_i^2 R + u_i \dot{\theta}_i), 0\} dt \ , \end{aligned} \tag{9}$$

where T is the duration of a stride. When performing negative work, part of the energy may be recovered with proper circuitry [2]. However, many robots – including SPEAR – do not have such capabilities; hence, we will assume that this part of the energy is eventually dissipated.

2) Cost of Hopping Forward: The cost of transport (COT) is a common metric for assessing the energy cost of locomotion. It measures the amount of energy required to transport a unit mass over a unit distance; mathematically,

$$c_{\text{cot}} = \frac{P}{Mgv} = \frac{c_{\text{ele}}}{MgvT} \ , \tag{10}$$

where M is the total weight of the robot and v is its average running velocity in one complete stride.

E. Optimization

To compare the energetic cost of realizing different gaits, a constrained optimization problem is formulated as follows

$$\begin{aligned} &\text{minimize} \quad c(z, \alpha) \\ &\text{such that} \quad z = \mathcal{P}(z, \alpha) \\ &\qquad\qquad \theta_{\text{hip}} \in [-70^\circ, 70^\circ] \ , \ \theta_{\text{knee}} \in [0^\circ, 140^\circ] \end{aligned} \tag{11}$$

where $c = c_{\text{ele}}$ for hopping-in-place and $c = c_{\text{cot}}$ for the hopping forward gait. The optimization problem (11) is solved numerically using MATLAB's `fmincon`.

V. Optimized Hopping-in-place

To provide some intuition on the nature of the motion regarding energy consumption, this section discusses optimized hopping-in-place gaits in SPEAR.

A. Hopping-in-place: One Cycle

To obtain periodic hopping-in-place motions, two additional constrains are incorporated in (11), namely

$$x_{\text{hip}}(T) = x_{\text{hip}}(0) \quad \text{and} \quad \max_{t \in [0,T]} y_{\text{toe}}(t) = Y_{\text{toe}} \ , \tag{12}$$

where T is the duration of the gait and Y_{toe} is the maximum toe clearance. The first constraint in (12) ensures that there is no translation of the hip, while the second requires that the toe reaches a certain distance from the ground.

Figure 3 presents an optimized hopping gait corresponding to $Y_{\text{toe}} = 7.5$cm. As shown in Fig. 3(c)-3(d), during flight the knee joint flexes so that the toe reaches the desired clearance; this is realized by moving the lighter shank using the knee actuator, instead of hopping higher, which would incur additional energy cost. The evolution of the knee torque shown in Fig. 3(e) confirms these observations; the knee actuator first flexes the knee joint to reach the maximum clearance, then extends it to prepare for touchdown.

Moreover, Fig. 3(f) shows that both the knee and hip actuators perform mainly positive work, with negligible amount of negative work done during stance. Focusing in stance, it is clear from Fig. 3(e)-3(f) that the spring plays an important role in the energetic performance of the leg. It effectively stores energy during leg compression – note that the hip actuator contributes to this energy – and then releases this energy to prepare the leg for takeoff; it is only during the later part that the parallel knee actuator contributes by essentially "shaping" the response of the spring. To quantify the contribution of the spring to energy efficiency, let

$$\eta := 1 - \frac{\int_T \max(P_{\text{motor}}, 0)dt}{\int_T \max(P_{\text{joint}}, 0)dt} \ , \qquad (13)$$

where P_{motor} is the total power of the knee and hip motors, and P_{joint} is the mechanical power of the joints. The efficiency η was proposed in [18] as a metric of how much of the positive work in one stride is provided passively. For this gait, $\eta = 0.9$; i.e., 90% of the positive work at one stride is provided by the spring.

B. Energy Consumption and Stiffness Adjustment

It is evident from (1) that the knee angle at touchdown determines the rest angle of the rotational energy-storing knee spring, and as a result the effective stiffness of the leg during the ensuing stance phase. In more detail, the introduction of the switch that disengages the prismatic spring S_1 in the flight phase allows to freely determine the touchdown angle of the knee during flight *without* deforming S_1. Hence, at touchdown, the undeformed spring begins its compression from the knee angle that was specified during the previous flight phase, which can be different from one step to the next, depending on the control action. Note that the rotational spring at the knee joint can be viewed as a nonlinear virtual spring applied along the line connecting the hip and the toe [19]. Thus, changing the rest angle of the knee spring provides an effective mechanism for changing the stiffness of the virtual toe-to-hip spring; [8, Figure 4] presents more details on the corresponding virtual spring force–displacement relationship.

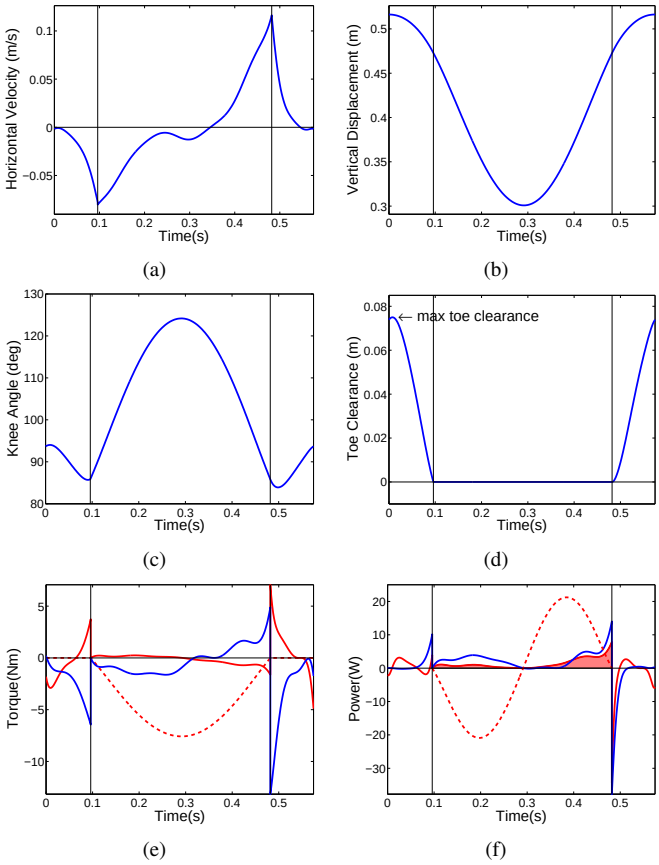

Fig. 3. Hopping-in-place for SPEAR. Vertical lines denote touchdown and liftoff. (a) Horizontal velocity of the hip. (b) Vertical displacement of the hip. (c) Knee angle. (d) Toe clearance. (e) Hip (blue solid), knee (red solid) and spring (red dotted) torques; the spring toque is scaled down by a factor of five. (f) Hip (blue solid), knee (red solid) and spring (red dotted) power; the spring power is scaled down by a factor of five.

The ability to tune the rest angle of the leg spring "cheaply" during the flight phase significantly influences energy consumption. To further investigate this effect we include an additional constraint $\theta^{\text{TD}}_{\text{knee}} = \Theta^{\text{TD}}_{\text{knee}}$ to the optimization problem defined by (12) and (11). Figure 4 presents the energetic cost for hopping with $Y_{\text{toe}} = 7.5$cm and for different touchdown angles $\Theta^{\text{TD}}_{\text{knee}}$. It can be seen that the cost is decreasing as the touchdown configuration of the knee is more bent. However, when the leg touches down in excessively "crouched" configurations, the energy cost starts increasing. This is attributed to the fact that, beyond a certain knee touchdown angle, the knee actuator performs negative work to decelerate the downward motion and prevent the leg from collapsing, thereby increasing the energy cost.

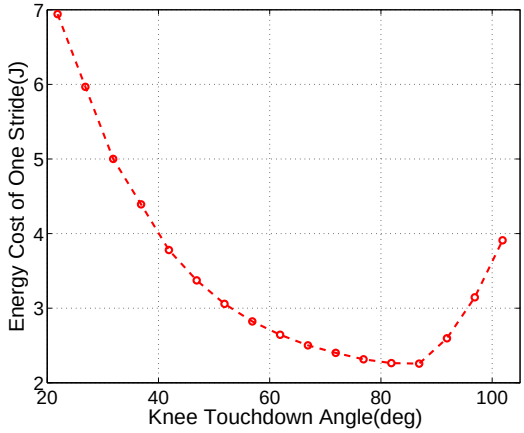

Fig. 4. The energy cost for hopping with a fixed maximum toe clearance of 7.5cm with different touchdown angles.

VI. Comparisons

In this section, we compare SPEAR with two alternative leg models; one model has a PEA at its knee joint but no switch and will be referred as the *PEA model*, and another model which has no spring and will be referred as the *rigid model*. For the PEA model, u_{spring} in (2) is given by

$$u_{\text{spring}} = -56.67 \ \max\{(\theta_{\text{knee}} - \bar{\theta}_{\text{knee}}), 0\} \ , \qquad (14)$$

where $\bar{\theta}_{\text{knee}}$ is the rest angle of the knee rotational spring. Due to the absence of the switch in the PEA model, $\bar{\theta}_{\text{knee}}$

cannot be adjusted; of course, the motor can modify the knee touchdown angle during flight, but such action necessarily deforms the spring. In what follows, we choose $\bar{\theta}_{\text{knee}} = 61°$, which is a compromise for different tasks as discussed at the end of this section. For the rigid model, the spring force u_{Pas} in (2) is zero. The parameters of the leg, as well as the controllers, are kept the same for the three models.

A. Hopping-in-place results

Figure 5 presents optimized hopping-in-place gaits for both the S-PEA and the PEA leg models obtained for different maximum toe clearances using the constraint sets (11) and (12). As Fig. 5(a) shows, while the energy cost is almost linearly increasing with the toe clearance, the PEA model uses 10-20% more energy than SPEAR. It can be seen in Fig. 5(b), that the optimizer favors motions in which the SPEAR flexes its knee joint actively in the flight phase to increase the toe clearance; this was also observed in Section V-A. However, the optimizer adopts a different strategy in the PEA leg model; this is due to the cost associated with flexing the knee during flight, where the knee actuator must perform work over the spring. Figure 5(c) shows that while the stride duration is increasing with the toe clearance, the stance phase duration is decreasing. From Fig. 5(d), it can be seen that the spring plays an important role in both models, providing more than 85% of the positive work used in one hopping stride.

In the case of the rigid model, the absence of a spring for storing mechanical energy and for reducing actuator torques – thus, reducing joule heating – dramatically increases energy consumption: compared to the SPEAR and PEA models, the rigid leg requires 33J per stride, which is about 14 times higher than the SPEAR model. Figure 6 indicates that the optimizer adopts a different energy-saving strategy for the rigid leg model. In flight, the leg quickly flexes the knee to satisfy the minimum toe clearance requirement. This strategy is similar to the optimized motions computed for the SPEAR model, due to the fact the two models behave in a similar fashion when the leg is in flight. In stance, however, the hip exhibits a much smaller vertical displacement: the vertical motion after touchdown is quickly brought to a stop at the first half of the stance phase. This is due to the fact that in the absence of an energy-storing spring, reducing the vertical displacement of the hip decreases the energy required by the actuators to maintain the motion. This is different from the PEA and SPEAR models.

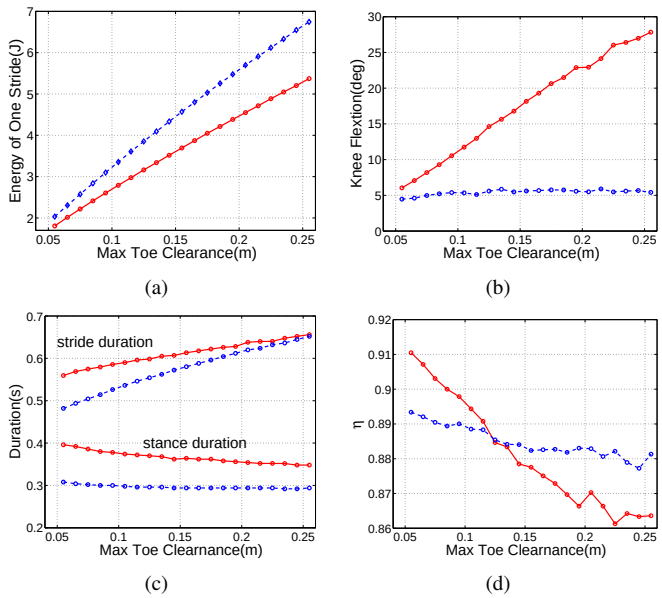

Fig. 5. Hopping-in-place gait for the SPEAR (red solid line) and for the PEA model (blue dashed line). (a) c_{ele} for different maximum toe clearances. (b) Maximum contraction of the knee angle at flight phase. (c) Stride and stance duration. (d) Hopping efficiency η computed by (13).

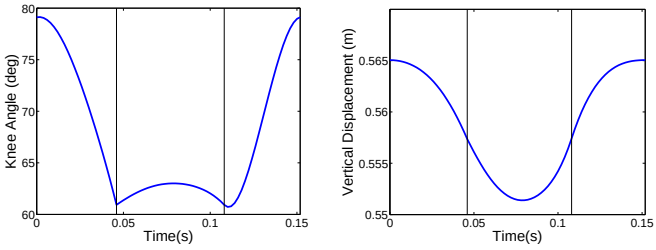

Fig. 6. Hopping-in-place for the rigid model. The maximum toe clearance is 7.5cm. The black vertical lines is the touchdown and liftoff event. (a) Knee angle. (b) Vertical displacement of hip.

B. Hopping-forward Results

Periodic forward hopping motions with different average velocities V_{aver} for the three models can be obtained by adding the constraint

$$v = \frac{x_{\text{hip}}(T) - x_{\text{hip}}(0)}{T} = V_{\text{aver}} \tag{15}$$

to the optimization constraint set in (11). Fig. 7 shows the COT, c_{cot}, computed by (10) for both the SPEAR and PEA models and for average velocities V_{aver} in the range from 0.2m/s to 4m/s. In both models, the COT decreases as velocity increases for relatively slow motions; however, after reaching a minimum value, the COT increases with the velocity. On average, the PEA model uses $10-20\%$ more energy compared to the SPEAR. This is increased to about 43% at 4m/s. Over the range $[1, 2]$ m/s, however, the COT of the PEA is comparable with that of the SPEAR.

The ability to tune the rest angle of the knee spring during flight without any energy cost explains part of the energetic advantage of the SPEAR over the PEA model. Figure 8 presents the knee touchdown angles of both the SPEAR and the PEA models for different desired toe clearances. For the SPEAR model, it is clear that the optimizer makes use of different touchdown angles (rest angles) to compute energy-efficient motions at different toe clearances. On the other hand, the optimizer avoids changing the knee touchdown angle in the PEA model due to the additional energy cost that is associated with deforming the knee spring during flight. Figure 8(b) shows that similar observations hold for forward hopping motions; the optimizer varies the knee touchdown angle of the SPEAR to realize energy efficient motions at

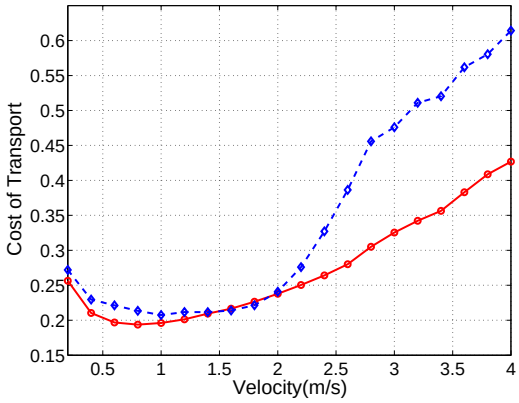

Fig. 7. COT of hopping at different velocities. The red line is for the SPEAR while the blue dashed line is for the PEA.

different forward velocities. In contrast, the knee touchdown angle does not vary significantly in the PEA model.

Finally, note that the rest angle $\bar{\theta}_{\text{knee}} = 61^\circ$ for the PEA is a compromise for the different running velocities and it is chosen as the rest angle of the SPEAR, when it runs at a medium velocity.

To summarize, the performance of the PEA can be comparable to that of the SPEAR, but only over a narrow range of velocities that are in the region where the knee touchdown angles in Fig. 8(b) of the SPEAR and PEA intersect – that is, at $1.5\text{m}/\text{s}$ where the COT for both models has a similar value, as Fig. 7 reveals. Note also that, although we do not optimize for actuator torque, the maximum torque for the S-PEA model is smaller than the PEA model, and the difference is increasing with running velocity. In general, the PEA design is outperformed by the SPEAR.

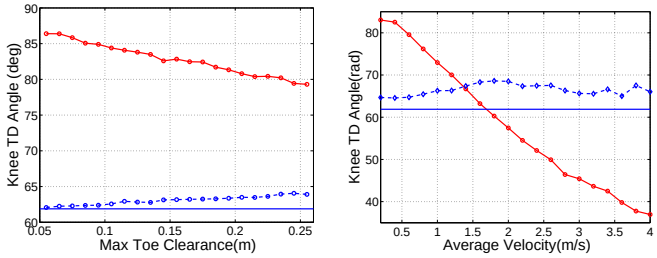

(a) (b)

Fig. 8. Knee touchdown angles for the SPEAR (solid red line) and the PEA model (blue dashed line). The blue horizontal line is the rest angle of the PEA model. (a) Hopping in place. (b) Hopping forward.

VII. Conclusion

Motivated by the Switchable Parallel Elastic Actuator (S-PEA) design recently proposed in [8] to actuate the knee joint of a monopedal robot, this paper investigates the implications of this design choice to energy consumption. Using parameter optimization, it is deduced that the introduction of a switch that isolates the energy-storing spring during flight – so that, (i) the leg configuration can be adjusted during flight without the motor interfering with the spring and (ii) part of the energy required to maintain the motion can be recycled during stance – significantly increases the performance of the system in terms of energy consumption. Through comparisons with alternative leg designs – one that includes a PEA without the switch and another that does not include compliance – it is shown that the S-PEA architecture exploits the advantages of both designs due to the fact that the effective stiffness of the S-PEA leg can be determined without any additional energy cost, simply by changing the knee touchdown angle during the flight phase.

References

[1] M. Raibert, K. Blankespoor, G. Nelson, R. Playter, and the BigDog Team, "BigDog, the rough-terrain quadruped robot," in *Proc. 17th IFAC World Congress*, Seoul, Korea, 2008, pp. 10 822–10 825.

[2] S. Seok, A. Wang, M. Y. Chuah, D. Otten, J. Lang, and S. Kim, "Design principles for highly efficient quadrupeds and implementation on the mit cheetah robot," in *Proc. IEEE Int. Conf. Robotics and Automation*, Karlsruhe, Germany, 2013, pp. 3307–3312.

[3] P. Holmes, R. J. Full, D. E. Koditschek, and J. Guckenheimer, "The dynamics of legged locomotion: models, analyses, and challenges," *SIAM Review*, vol. 48, no. 2, pp. 207–304, 2006.

[4] R. Alexander, *Elastic Mechanisms in Animal Movement*. Cambridge: Cambridge University Press, 1988.

[5] G. Pratt and M. Williamson, "Series elastic actuators," in *Proc. IEEE/RSJ Int. Conf. Intelligent Robots and Systems*, Pittsburgh, PA, 1995, pp. 399–406.

[6] K. Sreenath, H. Park, I. Poulakakis, and J. Grizzle, "A compliant hybrid zero dynamics controller for stable, efficient and fast bipedal walking on MABEL," *Int. J. Robotics Research*, vol. 30, no. 9, pp. 1170–1193, 2011.

[7] M. Plooij, M. van Nunspeet, M. Wisse, and H. Vallery, "Design and evaluation of the bi-directional clutched parallel elastic actuator (BIC-PEA)," in *Proc. IEEE Int. Conf. Robotics and Automation*, Seattle, USA, 2015, pp. 1002–1009.

[8] X. Liu, A. Rossi, and I. Poulakakis, "SPEAR: A monopedal robot with switchable parallel elastic actuator," in *Proc. IEEE/RSJ Int. Conf. Intelligent Robots and Systems*, Hamburg, Germany, 2015, pp. 5142–5147.

[9] U. Mettin, P. X. La Hera, L. B. Freidovich, and A. S. Shiriaev, "Parallel elastic actuators as control tool for preplanned trajectories of underactuated mechanical systems," *Int. J. Robotics Research*, vol. 29, no. 9, pp. 1186–1198, 2009.

[10] M. Grimmer, M. Eslamy, S. Gliech, and A. Seyfarth, "A comparison of parallel-and series elastic elements in an actuator for mimicking human ankle joint in walking and running," in *Proc. IEEE Int. Conf. Robotics and Automation*, 2012, pp. 2463–2470.

[11] G. A. Folkertsma, S. Kim, and S. Stramigioli, "Parallel stiffness in a bounding quadruped with flexible spine," in *Proc. IEEE/RSJ Int. Conf. Intelligent Robots and Systems*, Vilamoura, Portugal, 2012, pp. 2210–2215.

[12] D. F. Häufle, M. Taylor, S. Schmitt, and H. Geyer, "A clutched parallel elastic actuator concept: towards energy efficient powered legs in prosthetics and robotics," in *IEEE RAS/EMBS Int. Conf. Biomedical Robotics and Biomechatronics*, Roma, Italy, 2012, pp. 1614–1619.

[13] M. Plooij, G. Mathijssen, P. Cherelle, D. Lefeber, and B. Vanderborght, "Lock your robot: A review of locking devices in robotics," *IEEE Robotics Automation Magazine*, vol. 22, no. 1, pp. 106–117, 2015.

[14] J. Karssen, "Robotic bipedal running: Increasing disturbance rejection," Ph.D. dissertation, Delft University of Technology, 2013.

[15] C. Remy, K. Buffinton, and R. Siegwart, "Comparison of cost functions for electrically driven running robots," in *Proc. IEEE Int. Conf. Robotics and Automation*, Saint Paul, MN, 2012, pp. 2343–2350.

[16] Y. Yesilevskiy, W. Xi, and C. Remy, "A comparison of series and parallel elasticity in a monoped hopper," in *Proc. IEEE Int. Conf. Robotics and Automation*, Seattle, WA, 2015, pp. 1036–1041.

[17] E. R. Westervelt, J. W. Grizzle, C. Chevallereau, J. H. Choi, and B. Morris, *Feedback Control of Dynamic Bipedal Robot Locomotion*. Taylor & Francis/CRC Press, 2007.

[18] M. Hutter, C. D. Remy, M. A. Hoepflinger, and R. Siegwart, "Efficient and versatile locomotion with highly compliant legs," *IEEE/ASME Tr. Mechatronics*, vol. 18, no. 2, pp. 449–458, 2013.

[19] J. Rummel and A. Seyfarth, "Stable running with segmented legs," *Int. J. Robotics Research*, vol. 27, no. 8, pp. 919–934, 2008.